Oncogene (2020) 39:2612–2623
https://doi.org/10.1038/s41388-020-1169-8

ARTICLE

C3a elicits unique migratory responses in immature low-density neutrophils

Brian E. Hsu[1,2] · Joannie Roy[3,4] · Jack Mouhanna[5] · Roni F. Rayes[5] · LeeAnn Ramsay[1] · Sébastien Tabariès[1] · Matthew G. Annis[1] · Ian R. Watson[1,6] · Jonathan D. Spicer[5] · Santiago Costantino[3,4] · Peter M. Siegel[1,2,6]

Received: 22 May 2019 / Revised: 14 December 2019 / Accepted: 20 January 2020 / Published online: 4 February 2020

Abstract

Neutrophils represent the immune system's first line of defense and are rapidly recruited into inflamed tissue. In cancer associated inflammation, phenotypic heterogeneity has been ascribed to this cell type, whereby neutrophils can manifest anti- or pro-metastatic functions depending on the cellular/micro-environmental context. Here, we demonstrate that pro-metastatic immature low-density neutrophils (iLDNs) more efficiently accumulate in the livers of mice bearing metastatic lesions compared with anti-metastatic mature high-density neutrophils (HDNs). Transcriptomic analyses reveal enrichment of a migration signature in iLDNs relative to HDNs. We find that conditioned media derived from liver-metastatic breast cancer cells, but not lung-metastatic variants, specifically induces chemotaxis of iLDNs and not HDNs. Chemotactic responses are due to increased surface expression of C3aR in iLDNs relative to HDNs. In addition, we detect elevated secretion of cancer-cell derived C3a from liver-metastatic versus lung-metastatic breast cancer cells. Perturbation of C3a/C3aR signaling axis with either a small molecule inhibitor, SB290157, or reducing the levels of secreted C3a from liver-metastatic breast cancer cells by short hairpin RNAs, can abrogate the chemotactic response of iLDNs both in vitro and in vivo, respectively. Together, these data reveal novel mechanisms through which iLDNs prefentially accumulate in liver tissue harboring metastases in response to tumor-derived C3a secreted from the liver-aggressive 4T1 breast cancer cells.

Introduction

Neutrophils are the most abundant circulating leukocyte population in humans and play a key role in the innate immune response. They are rapidly recruited to sites of inflammation, where their role is to kill bacteria through phagocytosis, production of reactive oxygen species, release of anti-microbial granules and neutrophil extracellular traps (NETs). Neutrophil recruitment from circulation is a multistep process that involves tethering, rolling, adhesion, crawling, and transmigration. Once neutrophils have been recruited into tissues, diverse chemokines further guide them to the inflammatory site. These major cytokines and chemokines include pro-inflammatory mediators (IL-1β and TNF), Ccr1 ligands (Ccl3 and Ccl5), Cxcr2 ligands (Cxcl1 and Cxcl2), Complement 5a (C5a), and lipid mediators such as leukotriene B4 (LTB_4) [1]. These signals are not only necessary for neutrophil adhesion to endothelial cells, but also enable further recruitment to the inflammatory site [2]. C3a, a key product of complement activation, has been shown to stimulate chemotaxis and degranulation of mast cells and eosinophils, but failed to induce chemotaxis of

Supplementary information The online version of this article (https://doi.org/10.1038/s41388-020-1169-8) contains supplementary material, which is available to authorized users.

✉ Peter M. Siegel
peter.siegel@mcgill.ca

1 Goodman Cancer Research Centre, McGill University, Montréal, QC H3A 1A3, Canada

2 Department of Medicine, McGill University, Montréal, QC H3G 1Y6, Canada

3 Research Centre, Maisonneuve-Rosemont Hospital, Montréal, QC H1T 2M4, Canada

4 Biomedical Engineering Institute, University of Montréal, Montréal, QC H3C 3T5, Canada

5 Department of Surgery, Research Institute of the McGill University Health Center, Montréal, QC H4A 3J1, Canada

6 Department of Biochemistry, McGill University, Montréal, QC H3G 1Y6, Canada

mature neutrophils [3, 4]. However, recent studies have shown the contrary, where pharmacological inhibition with a C3a-receptor antagonist (C3aRA) in mice was able to reduce neutrophil recruitment in an arthritis model [5], and genetic deletion of $C3^{-/-}$ and $C3aR^{-/-}$ significantly reduced the infiltration of neutrophils to the brain following cerebral lipopolysaccharide (LPS) stimulation [6]. These differential effects of C3a on neutrophil function may be resolved by the recent observations describing significant neutrophil heterogeneity. Emerging evidence has revealed that, in the context of metastatic cancer progression, neutrophils represent a heterogeneous population of innate immune cells. Cancer associated neutrophils are defined according to their localization, morphology, maturity, density, and biological functions [7]. Infiltrating neutrophils exhibit either anti-tumorigenic (N1) or pro-tumorigenic (N2) phenotypes [8]. TGF-β has been shown to influence neutrophil plasticity and TGF-β inhibition can induce a shift toward a N1 phenotype [8]. Recently, distinct circulating neutrophil phenotypes in cancer have also been described. Low-density neutrophils (LDNs) and high-density neutrophils (HDNs) were characterized in a murine breast cancer model [9]. HDNs have a mature, segmented morphology, and exhibit anti-tumor phenotypes. In contrast, LDNs are a heterogeneous population of mature and immature (banded and ring-shaped) neutrophils, possessing pro-tumor phenotypes [9]. While some studies have shown that HDNs are better at migrating toward tumor-derived factors when compared with LDNs, due to differential expression of neutrophil chemotactic receptors (Cxcr1/Cxcr2) [9, 10], others have shown that, in an intestinal tumor model, tumor progression is correlated with the accumulation of LDNs and induction of NETs by the increased expression of complement 3a receptor (C3aR) on LDNs [11].

We have previously shown that immature low-density neutrophils (iLDNs) can promote, while HDNs suppress liver metastasis in a murine triple negative breast cancer model [12]. We have investigated the differential migration of iLDNs and HDNs toward factors produced by breast cancer cells capable of forming liver metastases. Using this system, we demonstrate that C3a produced by liver-metastatic breast cancer cells can preferentially induce the migration of iLDNs relative to HDNs, via C3aR expressed on iLDNs. Our data suggests that the C3a/C3aR axis can preferentially induce the migration of immature low-density neutrophils.

Results

iLDNs accumulate more efficiently, compared with HDNs, in metastasis bearing liver tissue

We have previously shown that mice bearing 4T1 breast cancer liver metastases exhibit an increase in the mobilization of peripheral blood LDNs from 5% in naïve, non-tumor bearing mice, to 30% in mice bearing liver metastases [12]. Functionally, infusion of purified HDNs results in a decrease in liver metastases; whereas, infusion of purified iLDNs promotes the formation of liver metastases. Furthermore, we show that iLDNs likely promote liver metastasis due to their metabolic flexibility, which allows them to perform pro-metastatic functions under glucose-limiting conditions [12]. To investigate the accumulation of iLDN and HDN populations into the liver parenchyma of mice bearing hepatic metastases, we infused iLDNs (PE-Ly6G) and HDNs (APC-Ly6G), via tail vein injection, at a 1:1 ratio into mice bearing established liver metastases (1-week post-splenic injection of tumor cells) (Fig. 1a). We have previously observed that iLDNs exhibit prolonged survival relative to HDNs when cultured beyond 2 h. To ensure that differential accumulation of infused neutrophils did not reflect differential survival, all images were taken 30 min to 2 h post-infusion [12]. Infusion of iLDNs and HDNs in naïve mice showed no difference in the ability of either population to accumulate in the liver (Fig. 1b). However, in mice bearing established liver metastases, we observed a two-fold increase in the number of iLDNs within the liver tissue when compared with HDNs (Fig. 1b, c). As a control, we also quantified the iLDN/HDN ratio in lungs of the same liver metastasis bearing mice, which revealed a 1:1 ratio of the two neutrophils populations (Fig. 1b). In addition, infusion of labeled iLDNs (CellTracker Red) and HDNs (CellTracker Blue) (Supplementary Fig. 1a) into mice bearing established lung metastases (1-week post tail vein injection of tumor cells) revealed no significant increase in the accumulation of iLDNs relative to HDNs in lung tissue (Supplementary Fig. 1b). To validate these observations, we isolated iLDNs and HDNs from the peripheral blood of liver metastasis bearing donor animals and labeled them with vital dyes (iLDNs: CellTracker Red; HDNs: CFSE). Labeled neutrophil populations were infused, via tail vein injection, at a 1:1 ratio into mice bearing established liver metastases (1-week post-splenic injection of tumor cells) (Fig. 1d). The number of iLDNs and HDNs were quantified by flow cytometry (Fig. 1e) and from immunofluorescence images captured from whole-mounted livers within 2 h post-infusion (Fig. 1f). Quantification by either flow cytometry or immunofluorescence revealed a 1.7-fold increase in the accumulation of iLDNs relative to HDNs, which is consistent with the results obtained from intravital imaging (Fig. 1b, c). Interestingly, we have previously shown that in mice bearing hepatic metastases, there is significant recruitment of $Ly6G^{+}$, and NE^{+} neutrophils surrounding the margin of the metastatic lesions [13]. Taken together, this data reveals that iLDNs isolated from mice bearing hepatic metastases exhibit increased accumulation into liver tissue compared with HDNs.

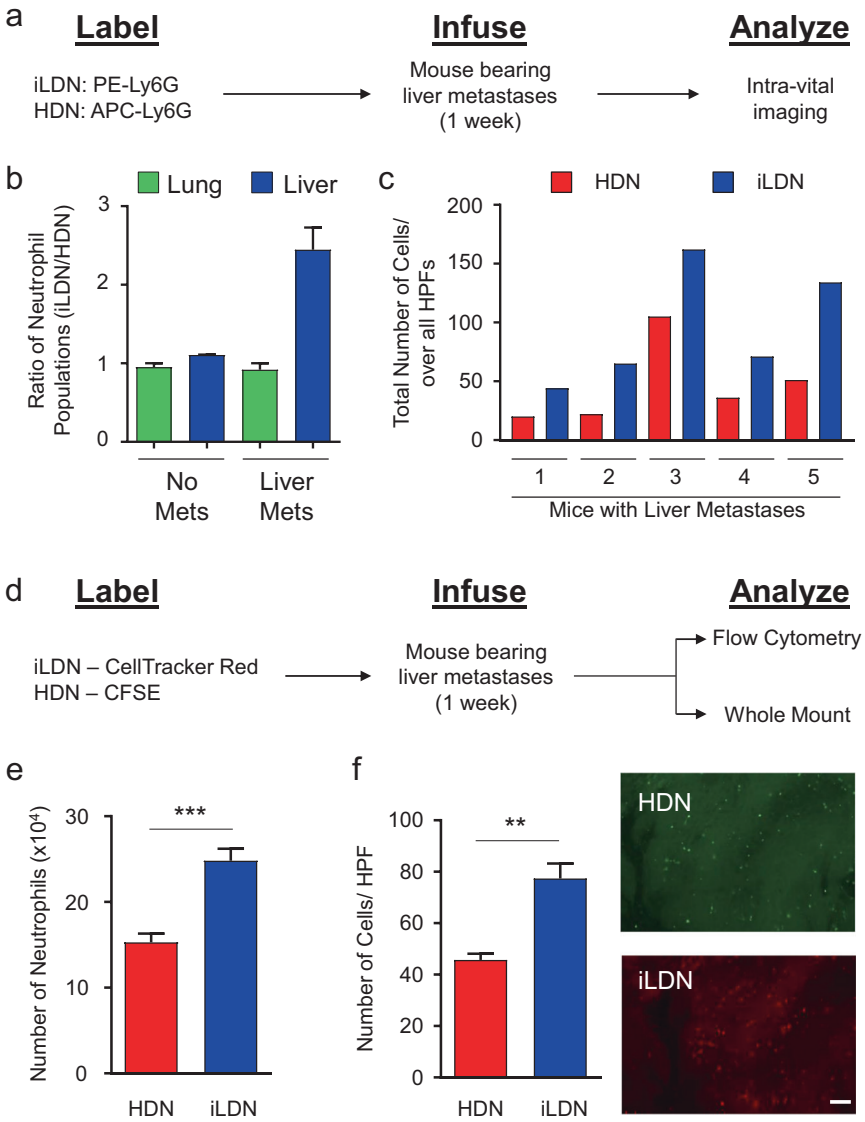

Fig. 1 iLDNs efficiently infiltrate metastasis bearing livers when compared with HDNs. a Schematic depicting how iLDN/HDN populations were differentially labeled with fluorescently conjugated antibodies prior to tail vein infusion (1:1 iLDN: HDN ratio) into mice bearing liver metastases (metastases established 1-week post-splenic injection with liver-aggressive 4T1 cells [2776]). Animals were subsequently subjected to intra-vital imaging of the liver. **b** Ratio of the average number of iLDNs/HDNs was plotted for non-metastasis bearing mice ($n = 2$) and mice bearing liver metastases ($n = 5$). Both the lungs and the livers were imaged for quantification 2 h following an infusion of a 1:1 mixture of iLDN: HDN populations by tail vein injection. **c** Total cell numbers quantified over all high-power fields (HPF; between 7 and 10) are plotted for HDNs and iLDNs. **d** Schematic of how iLDN and HDN populations were differentially labeled with vital dyes prior to tail vein infusion (1:1 iLDN: HDN ratio) into mice bearing liver metastases (1-week post injection). **e** Livers were harvested ($n = 5$ mice) and subjected to collagenase digestion followed by flow cytometry to quantify the number of $CFSE^+$ and $CellTrackerRed^+$ neutrophils. **f** Quantification of $CFSE^+$ and $CellTrackerRed^+$ neutrophils (per HPF; 5) by fluorescence microscopy of whole-mounted livers ($n = 5$ mice) is presented. Representative images of HPFs are shown. Scale bar represents 100 μm and applies to all images.

iLDNs preferentially migrate toward conditioned media derived from liver-metastatic breast cancer cells

One potential explanation for the increased accumulation of iLDNs, relative to HDNs, in metastasis bearing livers could be an enhanced ability of iLDNs to extravasate across sinusoidal endothelium and infiltrate the metastatic lesions within the liver. To explore this possibility, we interrogated RNA-Seq data generated from HDNs and iLDNs populations [12]. These analyses revealed that iLDNs exhibited an enrichment of genes relevant to leukocyte transendothelial migration

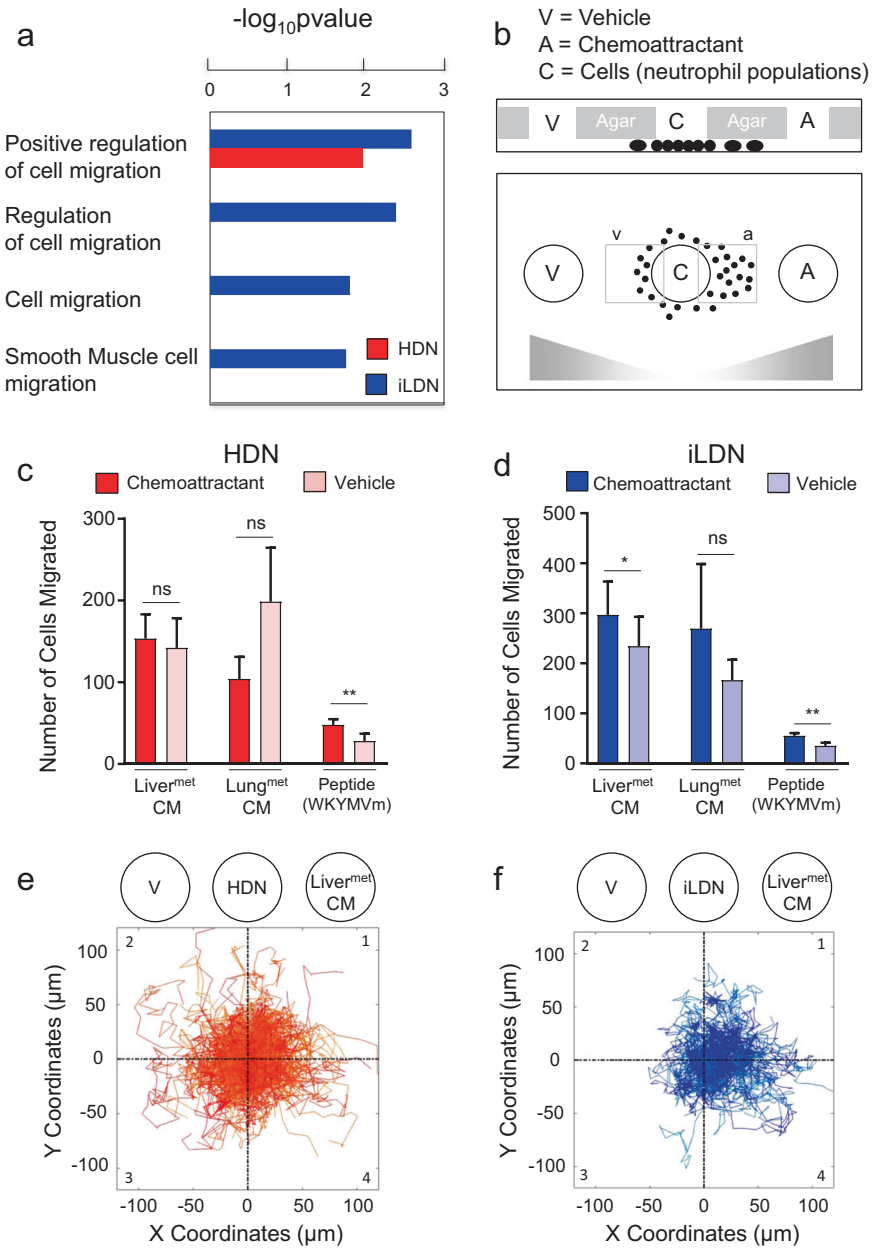

Fig. 2 iLDNs preferentially migrate toward conditioned media generated from liver-aggressive 4T1 breast cancer cells (2776). **a** Gene Ontology (GO) analysis using differentially expressed genes between iLDNs and HDNs with a fold change (FC) greater than 2 and examining migration enriched pathways. **b** Schematic illustrating neutrophil under agarose migration assays. Neutrophil populations were seeded in the central well (C) and the chemotactic agonist (chemoattractant) was placed on one side (A) while the vehicle solution was placed on the other side (V). Stable soluble gradients (gray triangles) are obtained within 15 min. The number of neutrophils that exited the central well toward either A or V within 2 h was measured. **c** The number of HDNs that migrated toward conditioned media from liver-metastatic breast cancer cells (Liver^{met} CM; $n = 9$ experiments), lung-metastatic breast cancer cells (Lung^{met} CM; $n = 4$ experiments) or a chemotactic peptide (WKYMVm; $n = 4$ experiments) relative to vehicle controls. n.s.: $P > 0.05$; $^{**}P \leq 0.01$, calculated using paired student's *t*-test. **d** The number of iLDNs that migrate toward conditioned media from liver-metastatic breast cancer cells (Liver^{met} CM; $n = 9$ experiments), lung-metastatic breast cancer cells (Lung^{met} CM; $n = 4$ experiments), or a chemotactic peptide (WKYMVm; $n = 4$ experiments) relative to vehicle controls. n.s.: $P > 0.05$; $^{*}P \leq 0.05$, $^{**}P \leq 0.01$ calculated using paired student's *t*-test. The trajectories of HDNs (**e**) or iLDNs (**f**) are represented after transposing the starting coordinate of each trajectory to a referential origin coordinate (0,0). These plots are tracks from one representative experiment.

(Supplementary Fig. 2a). RT-qPCR analysis of genes within this signature that are either induced (*Rapgef3, Mapk13, Pecam1*, and *Vasp*) or suppressed (*Icam1, Ezr, Plcg1*, and *Cxcr4*) confirmed a subset of components within this leukocyte transendothelial migration pathway are increased in iLDNs relative to HDNs (Supplementary Fig. 2b, c).

In addition to enhanced transendothelial migration, we hypothesized that mechanisms that control neutrophil migration were preferentially engaged in iLDNs, which resulted in their enhanced accumulation within metastasis bearing livers. Analysis of gene ontology terms from RNA-Seq (GSE123669) data revealed that cell migration processes are enriched in iLDNs compared with HDNs (Fig. 2a). To confirm differences in cell migration between iLDNs and HDNs, we used the under-agarose cell migration assay, which is a well-established technique for measuring neutrophil migration [14–26]. To measure neutrophil migration, we tested the ability of iLDNs and HDNs to respond to conditioned media produced from either the liver-aggressive (2776) or lung-aggressive (526) explants derived from 4T1 breast cancer cells [12]. Neutrophils were deposited in a central well (C) and were exposed to diffusion gradients that emanated from wells containing chemoattractants (A) or vehicle (V) (Fig. 2b). While HDNs failed to respond to conditioned media from either lung- or liver-metastatic breast cancer cells (Fig. 2c), iLDNs exhibited a migratory response specifically toward conditioned media harvested from liver-metastatic breast cancer cells (Fig. 2d). As a positive control, a chemotactic peptide (WKYMVm) was used that elicited migratory responses from both iLDNs and HDNs (Fig. 2c, d). We next evaluated dynamic responses of iLDNs and HDNs to conditioned media derived from liver-aggressive breast cancer cells. Representing individual neutrophil cell tracks from their origin, we observed that the trajectories of HDNs were uniformly distributed in all four quadrants, revealing that these neutrophils displayed no preferential chemotaxis toward conditioned media derived from liver-metastatic breast cancer cells relative to vehicle controls (Fig. 2e). In contrast, iLDNs are preferentially grouped within the first and fourth quadrant in response to conditioned media harvested from liver-metastatic breast cancer cells (Fig. 2f). These results can also be observed by representing each trajectory step on a polar histogram, where trajectory steps that localize strongly in angles 0° to 60° and in 300° to 360° indicate a migratory response corresponding to the gradient direction (Supplementary Fig. 3a). HDNs reveal a similar distribution of trajectory steps between these intervals in response to conditioned media from liver-metastatic breast cancer cells (34.46%; HDNs, CM) compared with vehicle controls (34.57%; HDNs, Veh.) (Supplementary Fig. 3a). In contrast, the data reveal a bias in iLDNs exposed to a gradient of conditioned media derived from liver-metastatic breast cancer cells, where 36.28% of the trajectory steps are contained within these intervals (iLDNs, CM) when compared with 34.46% of the trajectory steps within these intervals for iLDNs responding to vehicle controls (iLDNs, Veh.) (Supplementary Fig. 3a). We found that the forward migration index (FMI) for iLDNs responding to conditioned media from liver-aggressive breast cancer cells was significantly higher than iLDNs responding to vehicle (media) or HDNs responding to either conditioned media from liver-aggressive breast cancer cells or vehicle (Supplementary Fig. 3b). Finally, we calculated mean trajectory speeds for both iLDNs and HDNs in response to vehicle or conditioned media from liver-metastatic breast cancer cells. HDNs migrated faster relative to iLDNs when responding to either vehicle or conditioned media derived from liver-metastatic breast cancer cells (Supplementary Fig. 3c). While iLDNs migrated slower than HDNs, iLDNs responding to conditioned media from liver-metastatic breast cancer cells migrated faster relative to those exposed to vehicle (Supplementary Fig. 3c).

A C3a–C3aR axis is engaged in iLDNs that migrate toward conditioned media derived from liver-aggressive breast cancer cells

To determine the chemokine receptors that are differentially expressed between HDNs and iLDNs, we interrogated RNA-seq data for genes encoding leukocyte receptors involved in chemotaxis. Elevated expression levels of three receptors known to be involved in neutrophil chemotaxis were detected in iLDNs relative to HDNs (Fig. 3a). Leukotriene B4 receptor and CCR2 have been known to be involved in neutrophil chemotaxis [27, 28]; whereas, complement 3a receptor (C3aR1) is expressed on almost all myeloid cells and is involved in basophil and eosinophil chemotaxis [3, 4]. Neutrophils in homeostatic conditions have been shown to express very low levels of C3aR; however, upon lipopolysaccharide (LPS) stimulation, cell surface expression of C3aR can be upregulated [11, 29]. Interestingly, there have been a few reports illustrating that a C3aR inhibitor was able to inhibit neutrophil recruitment to sites of inflammation [5, 30–32]. The elevated expression of C3aR in iLDNs was also of particular interest as we detected a 1.7-fold increase in secreted C3a in the conditioned media from liver-metastatic (2776) breast cancer cells compared with parental 4T1 cells and a 9-fold increase when compared with lung-metastatic (526) breast cancer cells normalized by either protein concentration or cell number (Fig. 3b). The secretion of either C5a or LTB_4, in conditioned media harvested from 4T1, lung- or liver-metastatic breast cancer cells, was undetectable by ELISA (data not shown). Due to lack of commercially available mouse specific antibodies, we were unable to examine LTB4R expression on iLDNs and HDNs by flow cytometry. Flow cytometric analyses revealed that C3aR1 expression was 1.5-fold higher in iLDNs compared with HDNs; whereas, C5aR1 and CCR2 were equally expressed on both HDNs and iLDNs (Fig. 3c, d). Taken together, these data suggest a potential role for a C3a/C3aR axis in promoting the migration of iLDNs.

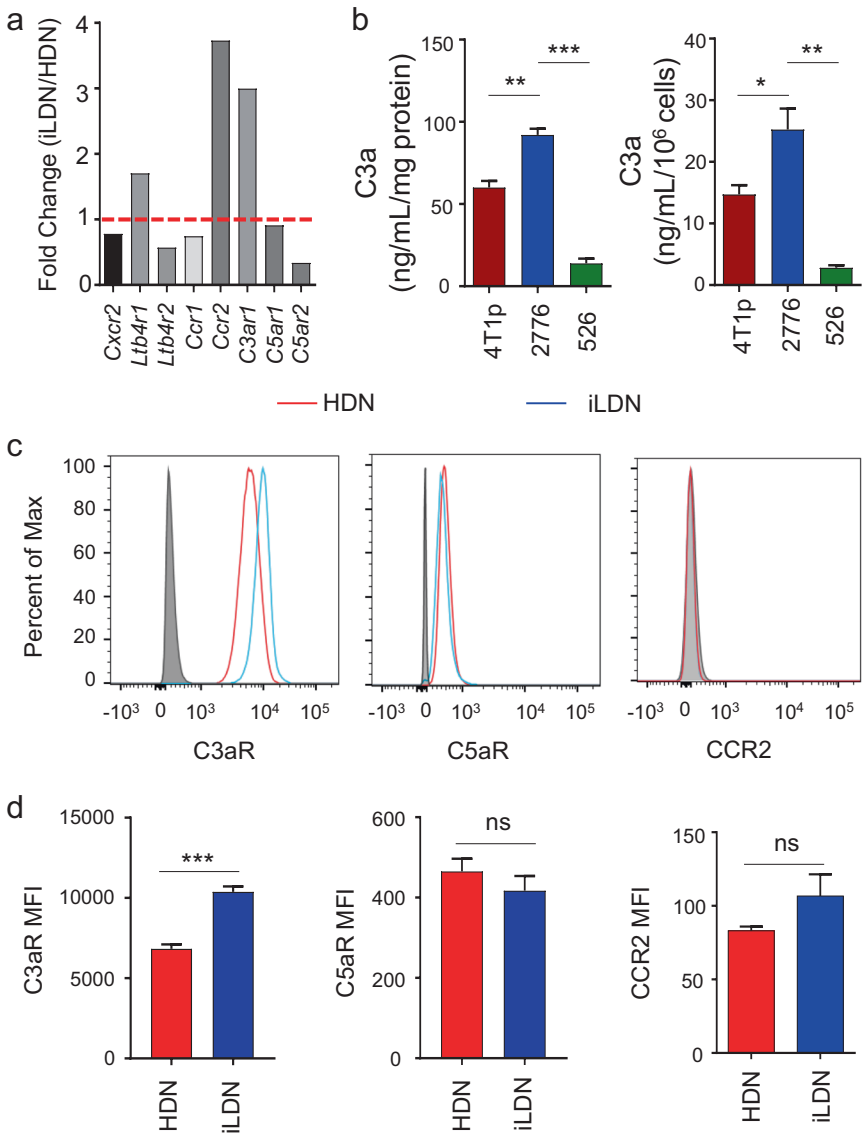

Fig. 3 C3a–C3aR axis is engaged in iLDNs migrating toward conditioned media derived from liver-aggressive 4T1 breast cancer cells (2776). a Average expression values of *Cxcr2*, *Ltb4r1*, *Ltb4r2*, *Ccr1*, *Ccr2, C3ar1*, *C5ar1*, and *C5ar2* obtained from RNA-Seq analyses are plotted as the fold change in expression between iLDNs and HDNs populations. **b** ELISA data for C3a detected in conditioned media collected from parental ($n = 3$), liver- ($n = 3$) and lung-metastatic ($n = 3$) 4T1 breast cancer cell populations normalized by protein concentration and cell number ($^*P \le 0.05$, $^{**}P \le 0.01$, $^{***}P < 0.001$). **c** Distinct HDNs (red) and iLDNs (blue) populations isolated from whole blood of mice bearing breast cancer liver metastases (2776) were analyzed for C3aR1, C5aR1, and Ccr2 cell surface expression. Histogram plots show expression of these receptors, compared with isotype control (black), in HDNs (red) and iLDNs (blue) populations. **d** The mean fluorescence intensity (MFI) of C3aR1, C5aR1, and Ccr2 in HDN and iLDN populations is shown ($n = 5$ mice/group for all graphs). ($^{***}P \le 0.001$).

Inhibition of C3aR blocks the preferential migration of iLDNs toward conditioned media derived from liver-metastatic breast cancer cells

To investigate whether elevated C3aR1 on the surface of iLDNs is functional, we tested whether recombinant C3a could specifically induce chemotaxis in iLDNs compared with HDNs. Indeed, the number of neutrophils that exhibited a specific chemotactic response toward C3a was higher in iLDNs compared with HDNs; whereas, both iLDNs and HDNs exhibited migratory responses to C5a (Fig. 4a, b). To determine the appropriate concentration of C3aR inhibitor (SB290157); 100 nM, 1 μM, and 10 μM were each individually tested for their impact on the chemotactic response of HDNs and iLDNs to C3a (Supplementary Fig. 4). Both 100 nM and 1 μM inhibited iLDN chemotaxis; resulting in similar numbers of iLDNs moving toward and away from C3a. In contrast, 10 μM of the C3aR inhibitor resulted in a greater number of iLDNs migrating away from C3a (chemo repulsion) (Supplemental Fig. 4). Therefore, a concentration

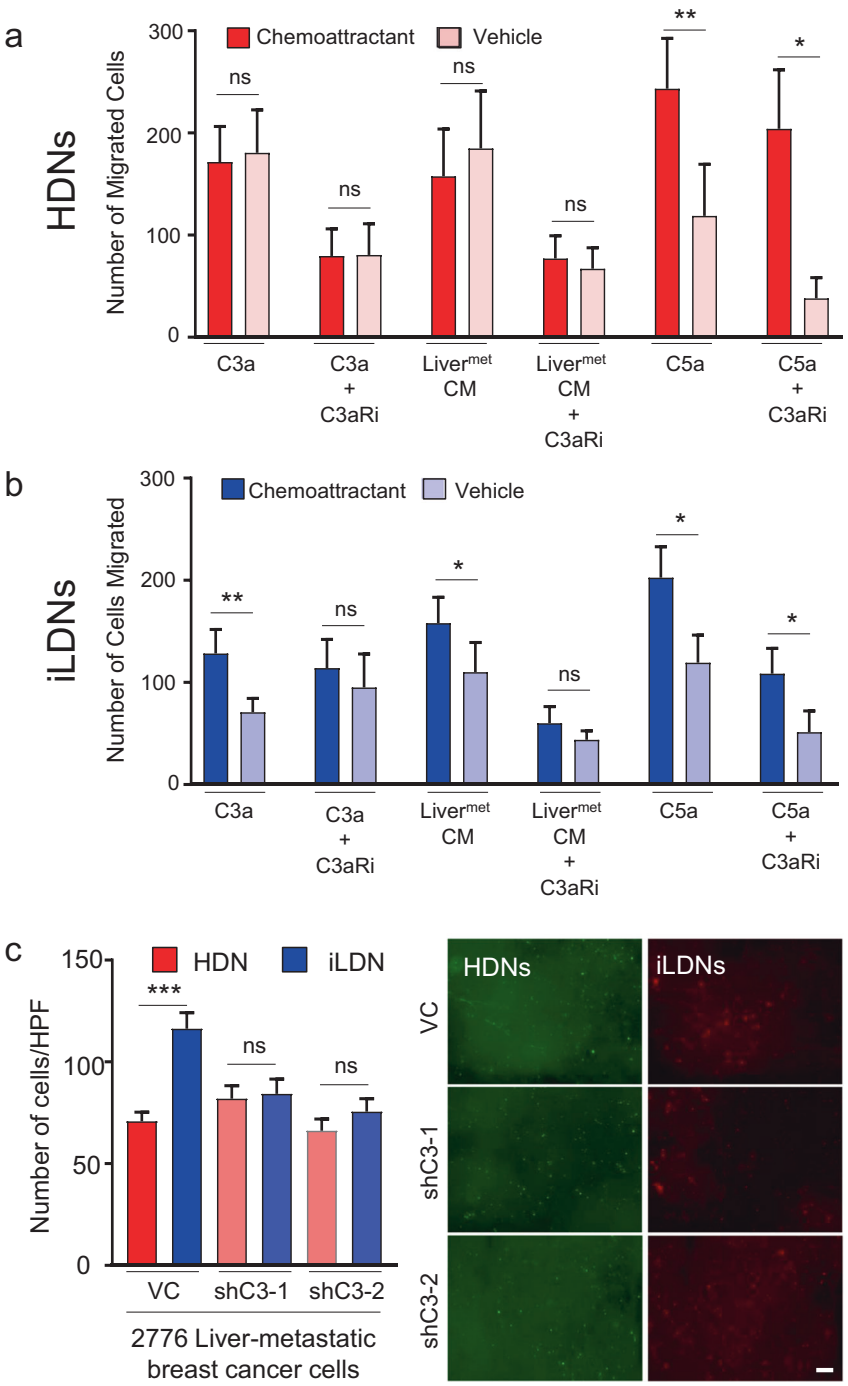

Fig. 4 Inhibition of C3aR blocks the preferential migration of iLDNs toward conditioned media derived from liver-aggressive 4T1 breast cancer cells (2776). a The number of HDNs that migrated toward C3a (1 μg/ml) ($n = 8$ experiments), C3a + SB290157 (1 μM) (C3a + C3aRi; $n = 9$ experiments), conditioned media from liver-metastatic breast cancer cells (Liver^{met} CM; $n = 9$ experiments), Liver^{met} CM + SB290157 (Liver^{met} CM + C3aRi) ($n = 11$), C5a (0.1 μg/ml) ($n = 6$, $^{**}P \le 0.01$) and C5a + SB290157 (C5a + C3aRi) ($n = 5$, $^{*}P \le 0.05$) over a 2 h period. **b** The number of iLDNs that migrated toward C3a (1 μg/ml) ($n = 8$ experiments, $^{**}P \le 0.01$), C3a + SB290157 (1 μM) (C3a + C3aRi; $n = 9$ experiments), conditioned media from liver-metastatic breast cancer cells (Liver^{met} CM; $n = 9$ experiments, $^{*}P \le 0.05$), Liver^{met} CM + SB290157 (Liver^{met} CM + C3aRi) ($n = 11$), C5a (0.1 μg/ml) ($n = 6$, $^{*}P \le 0.05$) and C5a + SB290157 (C5a + C3aRi) ($n = 5$, $^{*}P \le 0.05$) over a 2 h period. Statistical analysis was calculated using paired student's *t*-test. **c** iLDN and HDN populations were differentially labeled with vital dyes prior to tail vein infusion (1:1 iLDN: HDN ratio) into mice bearing liver metastases (1-week post-splenic injection of cancer cells) of vector control (VC) ($n = 6$, $^{***}P \le 0.001$), shC3-1 ($n = 6$), or shC3-2 ($n = 6$) expressing 2776 cells. Quantification of CFSE^{+} and CellTrackerRed^{+} neutrophils (per HPF; between 5 and 6) by fluorescence microscopy of whole-mounted livers is presented. Representative images of HPFs are shown. Scale bar represents 100 μm and applies to all images.

of 1 μM of the C3aR inhibitor was selected for subsequent experiments. The addition of a C3aR inhibitor abrogated the migratory response of iLDNs toward both recombinant C3a and conditioned media harvested from liver-metastatic breast cancer cells (Fig. 4b). The inhibitor was specific to C3aR and failed to inhibit migration of iLDNs or HDNs toward C5a (Fig. 4a, b). Since LTB4R1 mRNA levels were elevated in iLDNs relative to HDNs, we examined whether LTB_4 could preferentially stimulate the migration of iLDNs compared with HDNs. LTB_4, administered at 100 nM and 250 nM, induced neutrophil chemotaxis of both HDNs and iLDNs to the same extent (Supplementary Fig. 5a, b). To determine whether this C3a-C3aR1 axis was important in vivo, we first generated two independent short hairpin RNAs (shRNAs) that stably diminished C3a levels in the liver-metastatic cells (2776) by 14.9-fold and 3.8 fold, respectively, which reduces the amount of C3a below the levels produced by lung-metastatic cells (526) (Supplementary Fig. 6a). We next isolated iLDNs and HDNs from peripheral blood of liver metastasis bearing donor animals and labeled them with vital dyes (iLDNs: CellTracker Red; HDNs: CFSE) as described earlier. Labeled neutrophil populations were infused into mice bearing established liver metastases from vector control (VC), shC3-1, or shC3-2 expressing 2776 cells (1-week post-splenic injection with tumor cells). Quantification by immunofluorescence revealed a 1.64-fold increase in the accumulation of iLDNs relative to HDNs in mice injected with VC cells, whereas mice receiving the shC3-1 or shC3-2 cells lost this differential in iLDN accumulation within the liver (Fig. 4c). To determine whether the reduced accumulation of iLDNs within the livers of metastasis bearing mice, following reduction of C3, we injected mice with vector control (VC), shC3-1 or shC3-2 expressing 2776 liver-metastatic breast cancer cells. Reducing C3 production failed to impair liver metastasis (Supplementary Fig. 6b, c). Altogether, we show that C3a–C3aR axis is important to induce a chemotactic response in iLDNs by tumor-derived C3a secreted from liver-metastatic breast cancer cells.

Discussion

Neutrophils play many different roles during the growth of primary tumors and subsequent seeding/successful colonization of metastases at a distal site. Neutrophils exert anti-tumorigenic or pro-tumorigenic functions that are context-dependent. Here, we highlight the differential migratory functions of two neutrophil populations (HDNs and iLDNs) isolated from liver metastasis bearing mice. iLDNs, mobilized in mice bearing liver metastases, accumulate more efficiently within the liver when compared with their HDN counterparts. Two potential mechanisms may contribute to this observation, which include enhanced neutrophil transendothelial migration of iLDNs compared with HDNs. The second mechanism may reflect enhanced migrations of iLDNs toward liver-metastatic breast cancer cells compared with HDNs. Overall, cytokines and chemokines are necessary to promote the infiltration and recruitment to the liver-metastatic sites.

Chemotaxis toward cancer cell-derived factors is necessary to guide neutrophils to liver metastases following transendothelial migration. We show that iLDNs preferentially respond to conditioned media obtained from liver-metastatic compared with lung-metastatic breast cancer variants. Transcriptomic analyses of both HDNs and iLDNs reveal differential expression of several chemokine receptors. LTB_4 has previously been shown to be important in neutrophil swarming in sites of inflammation and recruitment in breast cancer [27, 33, 34]. The expression of *Ltb4r* is increased about two-fold at the mRNA level in iLDNs compared with HDNs; however, both neutrophil populations exhibited robust chemotaxis responses upon exposure to recombinant LTB_4.

Complement activation and generation of complement protein products, especially C3a and C5a have important roles in innate immunity. For example, C5a has been very well characterized as one of the most potent inflammatory peptides, which promotes chemotaxis of many different innate immune cells, including neutrophils [4, 35]. In addition, C5a also induces an oxidative burst and enhanced phagocytosis in neutrophils [36]. Indeed, in our studies, both iLDNs and HDNs were responsive to stimulation with C5a. In contrast, C3a has been shown to stimulate chemotaxis and degranulation of mast cells and eosinophils but fails to induce chemotaxis of mature neutrophils [3, 4]. Interestingly, there have been limited reports on the physiological function of C3aR in neutrophils despite the rapid rise in intracellular calcium following addition of low nanomolar concentrations of C3a [3]. The importance of C3aR function in neutrophils has recently been highlighted in mice predisposed to develop intestinal tumors ($APC^{Min/+}$). It was shown that low-density neutrophils (LDNs) were prone to produce NETs and that effect was dependent on C3aR [11]. The heterogeneity of neutrophils in cancer has made it difficult to precisely characterize these cells. By identifying neutrophils in the high- and low-density fractions [9], which possess anti- and pro-tumorigenic properties in liver metastasis respectively [12], we were able to investigate potential mechanisms of neutrophil migration.

In contrast to mature neutrophils, we show that iLDNs preferentially respond to conditioned media obtained from liver-metastatic compared with lung-metastatic breast cancer variants. Interestingly, the expression of C3aR was elevated at the mRNA level and displayed a 1.5-fold

increase in cell surface expression by flow cytometric analyses in iLDNs compared with HDNs. Moreover, recombinant C3a elicited a chemotaxis response in iLDNs but not HDNs, with the latter observation being consistent with previous reports [3]. This effect was abrogated following inhibition of C3aR with SB290157, which is a non-peptide antagonist of C3aR. In line with the iLDN response to C3a, the liver-metastatic breast cancer cells expressed higher levels of secreted C3a compared with parental 4T1 cells and the lung-aggressive breast cancer cells. This observation may explain why iLDNs better respond to conditioned media from liver-metastatic breast cancer cells compared with conditioned media from lung-metastatic breast cancer cells.

Our findings highlight the complexity of neutrophil heterogeneity. Two neutrophil populations, which both express $Ly6G^+$ and $CD11b^+$, only differ with respect to their maturation status and density. We show that the reduction of C3a was sufficient to reduce the recruitment of iLDNs to liver metastases. The reduction of C3a did not affect liver-metastatic burden at end-point; however, this result may not be entirely surprising. C3a has been shown to elicit both anti- and pro-inflammatory functions depending on the cell types involved and the degree of inflammation induced. C3a can increase the production of pro-inflammatory mediators, such as IL-1β and TNFα in monocytes/macrophages [37]. In addition, C3a has been shown to prolong the inflammatory response by suppressing regulatory T-cell production [38]. In chronic inflammation, such as rheumatoid arthritis and asthma, C3a has also been shown to have pro-inflammatory effects [39, 40]. All of these C3a mediated functions could result in an anti-tumor immune environment that would limit growth of the metastases. Thus, by reducing C3a levels in the liver-metastatic breast cancer cells, changes may occur in the tumor immune microenvironment that enable growth of the metastases that surpass the detrimental effects of impairing iLDN recruitment to the growing lesions.

In addition, with the identification of iLDNs as a subpopulation of neutrophils, it would be interesting to assess whether there are other chemoattractants or chemokine receptors that promote the accumulation of iLDNs into liver metastases. This would shed some light on which chemokines secreted by tumor cells can also promote recruitment and infiltration of pro-metastatic immature neutrophils.

In summary, our studies reveal that iLDNs, relative to HDNs, preferentially accumulate liver tissue bearing breast cancer metastases. Our in vitro assays revealed conditioned media from liver-, but not lung-, metastatic breast cancer cells promotes the migration of iLDNs. We identified that migration of iLDNs is due, in part, to elevated surface expression of C3aR1 on iLDN populations and chemotaxis toward C3a expressed by liver-metastatic breast cancer cells.

Materials and methods

Mice

Female Balb/c mice (6–8 weeks old) were purchased from Charles River. Mice were housed in facilities managed by the McGill University Animal Resources Center and all animal experiments were conducted under the McGill University-approved Animal Use Protocol (AUP#2012-5129). Randomization and blinding of mice were not conducted for the animal experiments. Protocols for live animal experiments were subjected to peer review for scientific merit, in accordance with guidelines established by the Canadian Council on Animal Care.

Cell culture and transfections

The 4T1 cell line was obtained from the American Type Culture Collection and cultured as previously described [41]. Isolation of 4T1 derived liver- (2776) and lung-metastatic (526) cell populations has been described previously [13]. Two independent shRNAs targeting C3 (TRCN0000348323, TRCN0000334476) were obtained from the TRC lentiviral shRNA library collection, kindly provided by the Genetic Perturbation Service (Goodman Cancer Research Centre, McGill University). 4T1 derived liver-metastatic cells (2776) with or without shRNAs targeting C3 (shC3-1/shC3-2) were injected via intrasplenic injections (1×10^5 cells) and 4T1 derived lung-metastatic cells (526) were used for intravenous injection (5×10^5 cells).

RNA isolation and real-time RT-qPCR

Total RNA was extracted from isolated $Ly6G^+/CD11b^+$ neutrophils and reverse transcribed as previously described [13]. Following the reverse transcription reaction, all samples were diluted 1:5 in ddH2O and subjected to real-time PCR analysis with FastStart Universal Probe Master (Roche, Cat. #: 04913914001). For all targets, the following cycling conditions were: 95 °C for 10 min, followed by 40 cycles each consisting of 95 °C for 15 s, 60 °C for 30 s and 72 °C for 45 s. Incorporation of SYBR Green dye into the PCR products was monitored using a Lightcycler 480 (Roche). Primers are listed in Table S1. Transcript expression was normalized to *Gapdh* mRNA levels and depicted as the fold change in iLDN compared with HDN populations.

Mouse neutrophil purification

Isolation of HDN and iLDN populations from peripheral blood has been previously described [9, 12]. The cell

suspension was diluted with 5 mL of PBS and loaded onto a discontinuous Histopaque gradient (Sigma, St-Louis, Missouri, USA). Cells were extracted from the high-density and low-density fractions. Red blood cells were subsequently eliminated by resuspending the cell suspension in BD PharmLyse (BD Biosciences, San Jose, California, USA), following the manufacturer's protocol. To purify neutrophils, cells from the HDF and LDF were stained with Ly6G and CD11b and sorted using the BD FACS Aria Fusion.

Flow cytometry

Fc receptors were blocked with CD16/32 (Biolegend, San Diego, California, USA Cat. #: 101301) and subsequent surface staining of the indicated cell populations was performed in FACS buffer (2% FBS in PBS) for 30 min on ice. Antibodies used for flow cytometry are listed in Table S2. Dead cells were identified following staining with LIVE/DEAD Fixable Aqua Dead Cell Stain Kit (ThermoFisher, Waltham, Massachusetts, USA, Cat. #: L34957). Data were acquired on a FACSCanto II (BD Biosciences) or a LSR Fortessa (BD Biosciences) cytometer and analysis performed using FlowJo software (Tree Star).

Under agar chemotaxis assay

A thin layer (~3 mm) of low-melting agarose (UltraPure) (ThermoFisher, Massachusetts, USA, Cat. # 16520050), prepared in RPMI 1640 medium supplemented with 3% FBS (Gibco), was poured onto BSA coated glass-bottom culture dishes (MatTek, Ashland, Massachusetts, USA). Following gel solidification, a surgical punch was used to remove a cylindrical piece of agarose (2 mm in diameter) to seed LDS751 dye-labeled neutrophils in a volume of 10 µl. Side wells were punched in the agarose at a distance of 2 mm from the central well, in which chemoattractant or vehicle was added. WKYMVM control peptide (Sigma, St-Louis, Missouri, USA, Cat# W4270), recombinant mouse C3a (R&D systems, Minneapolis, Minnesota, USA, Cat#: 8085-C3-025); mouse C5a (R&D systems, Minneapolis, Minnesota, USA Cat#: 2150-C5-025); mouse LTB_4 (Cayman Chemical, Ann Arbor, Michigan, USA Cat#: 20110) and SB290157 (Cayman Chemical, Ann Arbor, Michigan, USA, Cat#: 15783) were used for chemotaxis assays.

Tumor conditioned media generation and ELISA

Cell culture supernatants from parental 4T1 and 4T1-metastatic subpopulations were collected following 72 h of culture and used for 1) analysis of the indicated factors with ELISA kits [C3a (LS Bio, Seattle, Washington, USA, Cat#: LS-F4210); C5a (LS Bio, Seattle, Washington, USA, Cat#: LS-F24035), 2) detection of LTB_4 (Cayman Chemical, Ann Arbor, Michigan, USA Cat#: 520111)] or 3) chemotaxis assays.

Intravital microscopy

Mice were subjected to tail vein injections with equal numbers of fluorescently labeled HDNs and iLDNs and adhesion to liver sinusoids visualized after 30 min. The left lobe of the liver was positioned on a glass coverslip over the microscope objective and imaging performed using an LD SC PApo 10X objective on a Zeiss LSM-780-NLO laser scanning confocal microscope (Carl Zeiss, Toronto, ON, Canada) provided by the molecular imaging platform of the RI-MUHC (http://rimuhc.ca/molecular-imaging).

Neutrophil vital-dye labeling

HDNs were labeled with Vybrant CFDA SE Cell Tracer Kit (1:1000 dilution, 15 min at 37°C, ThermoFisher, Waltham, Massachusetts, USA, Cat. #: V12883) or CellTracker Blue CMAC (1:1000 dilution, 15 min at 37°C, Waltham, Massachusetts, USA, Cat. #: C2110). iLDNs were labeled with CellTracker Red CMTPX Dye (1:1000 dilution, 15 min at 37°C, Waltham, Massachusetts, USA, Cat. #: C34552). HDNs and iLDNs were injected (1:1 ratio) via tail vein into mice bearing liver or lung metastases. Livers or lungs were collected 2 h post-infusion, divided into portions and were (1) subjected to collagenase digestion and flow cytometry analysis to assess the ratio of CFDA-SE labeled to CellTrackerRed labeled cells and (2) whole-mounted for imaging analysis. The number of extravasated CFDA-SE or CellTracker Blue labeled HDNs and CellTracker Red iLDNs per high-power field was assessed using an inverted Zeiss Axiozoom.V16 microscope (Carl Zeiss, Toronto, ON, Canada).

Bioinformatics analyses

Analysis of leukocyte transendothelial migration signature —mmu04670

To evaluate enrichment of the leukocyte transendothelial migration signature in iLDN and HDN populations (GSE123669), we obtained the gene signature from Kyoto Encyclopedia of Genes and Genomes database. Pathway gene set enrichment analysis (GSEA) was performed with the gage (version 2.24.0) R Bioconductor package [42]. The essGene() function from the gage R package was used to extract the essential gene members driving the enrichment in the GSEA and visualized as a heatmap with the geneData ()function.

Quantification and statistical analysis

With in vivo studies, no animals were excluded from the analysis. Sample size for animal experiments were calculated to be five mice for each group at significance level alpha of 5%, a priori power 90% and estimated effect side (*d*) 2.1, using G*Power software [43]. Statistical analyses were performed using Prism software (Graphpad) or Matlab (Mathwork). Unless otherwise stated, for studies comparing differences between two groups, an unpaired Student's *t*-test was used. Data are presented as mean ± SEM. Differences were considered significant when $P \leq 0.05$ or are indicated as not significant. Image analysis, cell detection and track analysis is further described in the Supplementary text [44–48].

Data availability

The accession number for the RNA-sequencing data is GEO: GSE123669. All informatics analyses were performed with R, an open source software environment for statistical computer and graphics. The software is available for download at https://cran.r-project.org/. Chemotaxis analyses were performed in Matlab (Mathwork). Further details are presented in the supplementary data.

Acknowledgements We acknowledge the Goodman Cancer Research Centre histology core facility (McGill University) for routine histological services, the Cell Vision Core Facility (McGill University) for providing routine cell sorting service and the Genetics Perturbation Service for shRNAs (McGill University). We thank Anie Monast and Cynthia Lavoie for technical support and members of the Siegel laboratory for their thoughtful discussions and critical reading of the manuscript. This work was supported by an operating grant to P.M.S. from the Cancer Research Society and the Terry Fox Research Institute and Québec Breast Cancer Foundation (Grant #: 242122). S.C. acknowledges funding support from NSERC and Genome Canada and salary awarded from FRQS. J.D.S acknowledges funding support from AATS, MGH foundation and FRQS. BEH acknowledges support from the Charlotte and Leo Karassik Foundation PhD Fellowship and the Rolande and Marcel Gosselin Graduate Studentship. PMS is a McGill University William Dawson Scholar.

Author contributions Conceptualization, BEH, JR, JDS, SC, PMS; Methodology, BEH, JR, JM, ST, JDS, SC, PMS; Validation, BEH, JR, ST, JM, RFR; Formal analysis, BEH, JR, ST, JM, RFR, LR, JDS, SC, PMS; Investigation, BEH, JR, ST; Resources, BEH, JR, JM, RFR, ST, MGA, IRW, JDS, SC, PMS; Data Curation, BEH, JR, JM, RFR, ST; Writing-Original Draft, BEH, JR, PMS; Writing-Review & Editing, BEH, JR, SC, PMS; Visualization, BEH, JR, LR, PMS; Supervision, ST, SC, PMS; Project administration, PMS; Funding acquisition, PMS.

Compliance with ethical standards

Conflict of interest The authors declare that they have no conflict of interest.

References

1. Sadik CD, Kim ND, Luster AD. Neutrophils cascading their way to inflammation. Trends Immunol. 2011;32:452–60.
2. Kolaczkowska E, Kubes P. Neutrophil recruitment and function in health and inflammation. Nat Rev Immunol. 2013;13:159.
3. Daffern PJ, Pfeifer PH, Ember JA, Hugli TE. C3a is a chemotaxin for human eosinophils but not for neutrophils. I. C3a stimulation of neutrophils is secondary to eosinophil activation. J Exp Med. 1995;181:2119.
4. Hartmann K, Henz BM, Krüger-Krasagakes S, Köhl J, Burger R, Guhl S, et al. C3a and C5a stimulate chemotaxis of human mast cells. Blood. 1997;89:2863.
5. Hutamekalin P, Takeda K, Tani M, Tsuga Y, Ogawa N, Mizutani N, et al. Effect of the C3a-receptor antagonist SB 290157 on anti-OVA polyclonal antibody-induced arthritis. J Pharm Sci. 2010;112:56–63.
6. Wu MC, Brennan FH, Lynch JP, Mantovani S, Phipps S, Wetsel RA, et al. The receptor for complement component C3a mediates protection from intestinal ischemia-reperfusion injuries by inhibiting neutrophil mobilization. Proc Natl Acad Sci USA. 2013;110:9439–44.
7. Mishalian I, Granot Z, Fridlender ZG. The diversity of circulating neutrophils in cancer. Immunobiology. 2017;222:82–8.
8. Fridlender ZG, Sun J, Kim S, Kapoor V, Cheng G, Ling L, et al. Polarization of tumor-associated neutrophil phenotype by TGF-beta: "N1" versus "N2" TAN. Cancer Cell. 2009;16:183–94.
9. Sagiv JY, Michaeli J, Assi S, Mishalian I, Kisos H, Levy L, et al. Phenotypic diversity and plasticity in circulating neutrophil subpopulations in cancer. Cell Rep. 2015;10:562–73.
10. Brandau S, Trellakis S, Bruderek K, Schmaltz D, Steller G, Elian M, et al. Myeloid-derived suppressor cells in the peripheral blood of cancer patients contain a subset of immature neutrophils with impaired migratory properties. J Leukoc Biol. 2011;89:311–7.
11. Guglietta S, Chiavelli A, Zagato E, Krieg C, Gandini S, Ravenda PS, et al. Coagulation induced by C3aR-dependent NETosis drives protumorigenic neutrophils during small intestinal tumorigenesis. Nat Commun. 2016;7:11037.
12. Hsu BE, Tabaries S, Johnson RM, Andrzejewski S, Senecal J, Lehuede C, et al. Immature low-density neutrophils exhibit metabolic flexibility that facilitates breast cancer liver metastasis. Cell Rep. 2019;27:3902–e6.
13. Tabariès S, Ouellet V, Hsu BE, Annis MG, Rose AA, Meunier L, et al. Granulocytic immune infiltrates are essential for the efficient formation of breast cancer liver metastases. Breast Cancer Res. 2015;17:45.
14. Nelson RD, Quie PG, Simmons RL. Chemotaxis under agarose: a new and simple method for measuring chemotaxis and spontaneous migration of human polymorphonuclear leukocytes and monocytes. J Immunol. 1975;115:1650–6.
15. Palmblad J, Malmsten CL, Udén AM, Rådmark O, Engstedt L, Samuelsson B. Leukotriene B4 is a potent and stereospecific stimulator of neutrophil chemotaxis and adherence. Blood. 1981;58:658–61.
16. Krauss AH, Nieves AL, Spada CS, Woodward DF. Determination of leukotriene effects on human neutrophil chemotaxis in vitro by differential assessment of cell motility and polarity. J Leukoc Biol. 1994;55:201–8.
17. Foxman EF, Campbell JJ, Butcher EC. Multistep navigation and the combinatorial control of leukocyte chemotaxis. J Cell Biol. 1997;139:1349–60.

18. Foxman EF, Kunkel EJ, Butcher EC. Integrating conflicting chemotactic signals. The role of memory in leukocyte navigation. J Cell Biol. 1999;147:577–88.
19. Heit B, Tavener S, Raharjo E, Kubes P. An intracellular signaling hierarchy determines direction of migration in opposing chemotactic gradients. J Cell Biol. 2002;159:91–102.
20. Heit B, Kubes P. Measuring chemotaxis and chemokinesis: the under-agarose cell migration assay. Sci STKE. 2003;2003:Pl5.
21. Liu L, Das S, Losert W, Parent CA. mTORC2 regulates neutrophil chemotaxis in a cAMP- and RhoA-dependent fashion. Dev Cell. 2010;19:845–57.
22. Majumdar RA, Tameh T, Parent CA. Exosomes mediate LTB4 release during neutrophil chemotaxis. PLoS Biol. 2016;14: e1002336.
23. Saha P, Yeoh BS, Olvera RA, Xiao X, Singh V, Awasthi D, et al. Bacterial siderophores hijack neutrophil functions. J Immunol. 2017;198:4293–303.
24. Roy J, Mazzaferri J, Filep JG, Costantino S. A haptotaxis assay for neutrophils using optical patterning and a high-content approach. Sci Rep. 2017;7:2869.
25. Subramanian BC, Moissoglu K, Parent CA. The LTB4-BLT1 axis regulates the polarized trafficking of chemoattractant GPCRs during neutrophil chemotaxis. J Cell Sci. 2018;131:18.
26. Saunders CA, Majumdar R, Molina Y, Subramanian BC, Parent CA. Genetic manipulation of PLB-985 cells and quantification of chemotaxis using the underagarose assay. Methods Cell Biol. 2019;149:31–56.
27. Afonso PV, Janka-Junttila M, Lee YJ, McCann CP, Oliver CM, Aamer KA, et al. LTB4 is a signal-relay molecule during neutrophil chemotaxis. Dev Cell. 2012;22:1079–91.
28. Talbot J, Bianchini FJ, Nascimento DC, Oliveira RD, Souto FO, Pinto LG, et al. CCR2 expression in neutrophils plays a critical role in their migration into the joints in rheumatoid arthritis. Arthritis Rheumatol. 2015;67:1751–9.
29. Quell KM, Karsten CM, Kordowski A, Almeida LN, Briukhovetska D, Wiese AV, et al. Monitoring C3aR expression using a floxed tdTomato-C3aR reporter knock-in mouse. J Immunol. 2017;199:688–706.
30. Mizutani N, Nabe T, Yoshino S. Complement C3a regulates late asthmatic response and airway hyperresponsiveness in mice. J Immunol. 2009;183:4039.
31. Lohman RJ, Hamidon JK, Reid RC, Rowley JA, Yau MK, Halili MA, et al. Exploiting a novel conformational switch to control innate immunity mediated by complement protein C3a. Nat Commun. 2017;8:351.
32. Ames RS, Lee D, Foley JJ, Jurewicz AJ, Tornetta MA, Bautsch W, et al. Identification of a selective nonpeptide antagonist of the anaphylatoxin C3a receptor that demonstrates antiinflammatory activity in animal models. J Immunol. 2001;166:6341–8.
33. Lämmermann T, Afonso PV, Angermann BR, Wang JM, Kastenmüller W, Parent CA. Neutrophil swarms require LTB4 and integrins at sites of cell death in vivo. Nature. 2013;498:371–5.
34. Wculek SK, Malanchi I. Neutrophils support lung colonization of metastasis-initiating breast cancer cells. Nature. 2015;528:413–7.
35. Marder SR, Chenoweth DE, Goldstein IM, Perez HD. Chemotactic responses of human peripheral blood monocytes to the complement-derived peptides C5a and C5a des Arg. J Immunol. 1985;134:3325–31.
36. Mollnes TE, Brekke OL, Fung M, Fure H, Christiansen D, Bergseth G, et al. Essential role of the C5a receptor in E coli-induced oxidative burst and phagocytosis revealed by a novel lepirudin-based human whole blood model of inflammation. Blood. 2002;100:1869–77.
37. Takabayashi T, Vannier E, Clark BD, Margolis NH, Dinarello CA, Burke JF, et al. A new biologic role for C3a and C3a desArg: regulation of TNF-alpha and IL-1 beta synthesis. J Immunol. 1996;156:3455–60.
38. Lim H, Kim YU, Drouin SM, Mueller-Ortiz S, Yun K, Morschl E, et al. Negative regulation of pulmonary Th17 responses by C3a anaphylatoxin during allergic inflammation in mice. PLoS One. 2012;7:e52666.
39. Bautsch W, Hoymann HG, Zhang Q, Meier-Wiedenbach I, Raschke U, Ames RS, et al. Cutting edge: guinea pigs with a natural C3a-receptor defect exhibit decreased bronchoconstriction in allergic airway disease: evidence for an involvement of the C3a anaphylatoxin in the pathogenesis of asthma. J Immunol. 2000;165:5401–5.
40. Banda NK, Hyatt S, Antonioli AH, White JT, Glogowska M, Takahashi K, et al. Role of C3a receptors, C5a receptors, and complement protein C6 deficiency in collagen antibody-induced arthritis in mice. J Immunol. 2012;188:1469–78.
41. Tabariès S, Dong Z, Annis MG, Omeroglu A, Pepin F, Ouellet V, et al. Claudin-2 is selectively enriched in and promotes the formation of breast cancer liver metastases through engagement of integrin complexes. Oncogene. 2011;30:1318–28.
42. Luo W, Friedman MS, Shedden K, Hankenson KD, Woolf PJ. GAGE: generally applicable gene set enrichment for pathway analysis. BMC Bioinform. 2009;10:161
43. Faul F, Erdfelder E, Buchner A, Lang AG. Statistical power analyses using G*Power 3.1: tests for correlation and regression analyses. Behav Res Methods. 2009;41:1149–60.
44. Crocker JC, Grier DG. Methods of digital video microscopy for colloidal studies. J Colloid Interface Sci. 1996;179:298–310. 496.
45. Otsu N. A threshold selection method from gray-level histograms. IEEE Trans Syst Man Cybern. 1979;9:62–6.
46. Jaqaman K, Loerke D, Mettlen M, Kuwata H, Grinstein S, Schmid SL, et al. Robust single- particle tracking in live-cell time-lapse sequences. Nat Methods. 2008;5:695–702.
47. Mazzaferri J, Roy J, Lefrancois S, Costantino S. Adaptive settings for the nearest-neighbor particle tracking algorithm. Bioinformatics. 2015;31:1279–85.
48. Rink I, Rink J, Helmer D, Sachs D, Schmitz K. A haptotaxis assay for leukocytes based on surface-bound chemokine gradients. J Immunol. 2015;194:5549–58.